*J Neurophysiol* 95: 3191–3198, 2006.
First published February 1, 2006; doi:10.1152/jn.01309.2005.

# Vesicle Depletion and Synaptic Depression at a Mammalian Ribbon Synapse

**Joshua H. Singer and Jeffrey S. Diamond**
*Synaptic Physiology Unit, National Institute of Neurological Disorders and Stroke, National Institutes of Health, Bethesda, Maryland*

Submitted 13 December 2005; accepted in final form 24 January 2006

**Singer, Joshua H. and Jeffrey S. Diamond.** Vesicle depletion and synaptic depression at a mammalian ribbon synapse. *J Neurophysiol* 95: 3191–3198, 2006. First published February 1, 2006; doi:10.1152/jn.01309.2005. We estimated the size of the readily releasable pool (RRP) of vesicles at a ribbon synapse in the rat retina by making paired voltage-clamp recordings from presynaptic rod bipolar cells (RBCs) and postsynaptic AII amacrine cells in an in vitro retinal slice preparation. The RRP at each active zone was estimated to constitute seven vesicles, in the range of estimated RRP sizes at conventional synapses. During sustained presynaptic $Ca^{2+}$ entry, the RRP could be released with a time constant of about 4 ms. This ribbon synapse exhibited pronounced paired-pulse depression (PPD), which was attributable primarily to vesicle depletion. Recovery from PPD was slow ($\tau \approx 4$ s) but could be accelerated by increasing the duration of the depressing stimulus. The small RRP and very high release probability likely contribute to the transient characteristics of neurotransmission at RBC synapses.

## INTRODUCTION

Only a small subset of the vesicles contained within a synaptic terminal is available for exocytosis after $Ca^{2+}$ influx; these vesicles compose the so-called readily releasable pool (RRP). After a vesicle in the RRP undergoes exocytosis, the vacant release site is reoccupied after some time by a vesicle new to the RRP. The rates at which the RRP is depleted and replenished help to determine how synaptic strength varies with activity (Rizzoli and Betz 2005).

In the synaptic terminals of sensory neurons that signal by graded membrane potential changes, some portion of the vesicles is clustered around a protein structure called a synaptic ribbon (Sterling and Matthews 2005). In electron micrographs, the ribbon appears as a planar structure perpendicular to the plasma membrane and rows of vesicles are assembled on each of its two faces. Consequently, the ribbon is thought to be the organizing site for exocytosis: the RRP is thought to constitute the bottom rows of vesicles on either side of the membrane, and it has been suggested that the other ribbon-associated vesicles move down the ribbon as if on a conveyor belt to refill release sites as they become vacant (Mennerick and Matthews 1996; Neves and Lagnado 1999; von Gersdorff et al. 1996; but see Parsons and Sterling 2003).

Capacitance measurements of exocytosis from isolated goldfish Mb1 bipolar cell terminals yield a good agreement between the number of ribbon-associated vesicles visualized by electron microscopy and the number of vesicles that can undergo exocytosis after a 200-ms presynaptic depolarization (von Gersdorff et al. 1996). Capacitance measurements, however, cannot determine whether exocytosed vesicles are filled with transmitter and released into functioning synapses, nor can they readily detect the release of single vesicles. To circumvent these limitations, we made simultaneous, paired voltage-clamp recordings from synaptically coupled rod bipolar cells (RBCs) and AII amacrine cells in a mammalian retinal slice preparation to measure the RRP and examine how it changes during synaptic transmission. We found that the RRP in rat RBC terminals is small, rapidly depleted, and slowly refilled, making the synapses very sensitive to synaptic depression arising from vesicle depletion.

## METHODS

Experiments were performed at about 22°C in light-adapted, 200-$\mu$m tissue slices prepared from midtemporal retinas of Sprague–Dawley rats (P15–25) as described previously (Singer and Diamond 2003). Retinas were isolated in room-temperature artificial cerebrospinal fluid (ACSF) bubbled with 95% $O_2$-5% $CO_2$ and containing (in mM): 119 NaCl, 23 $NaHCO_3$, 10 glucose, 1.25 $NaH_2PO_4$, 2.5 KCl, 2.5 $CaCl_2$, 1.5 $MgCl_2$, 2 Na-lactate, and 2 Na-pyruvate. Isolated tissue was embedded in low-melting-point agarose (4% in ACSF with HEPES substituted for $NaHCO_3$ and Na-lactate and Na-pyruvate omitted) and slices were cut on a vibratome (Vibratome). Slices were stored and recordings made in this same ACSF bubbled with 95% $O_2$-5% $CO_2$.

Neurons were visualized by IR-DIC video microscopy. Whole cell recordings from AIIs were made using pipettes (about 5 MΩ) containing (in mM): 90 $CsCH_3SO_3$, 20 TEA-Cl, 10 HEPES, 10 EGTA, 10 mM Na-phosphocreatine, 4 MgATP, and 0.4 NaGTP. Holding potentials were corrected for an approximately 10-mV junction potential. Perforated-patch and whole cell recordings (7- to 15-MΩ pipettes) were made from RBCs. Unless indicated otherwise, the presynaptic internal solution contained (in mM): 90 $CsCH_3SO_3$, 20 TEA-Cl, 10 HEPES, 10 glutamic acid, 10 mM Na-phosphocreatine, 4 MgATP, and 0.4 NaGTP. For perforated-patch recordings, 0.2 mM EGTA and 0.5 mg/ml amphotericin B (water-soluble formulation) were included; for whole cell RBC recordings, 1.5 mM BAPTA was added. Postsynaptic access resistance was <20 MΩ and compensated 70–95%. Presynaptic access resistance was generally 25–50 MΩ and not compensated.

Recordings were made in ACSF containing picrotoxin (100 $\mu$M), TPMPA (50 $\mu$M), strychnine (0.5 $\mu$M), and tetrodotoxin (TTX, 0.25 $\mu$M) to block $\gamma$-aminobutyric acid type A ($GABA_A$) receptor–, $GABA_C$ receptor–, glycine receptor–, and voltage-gated $Na^+$ channel–mediated currents, respectively. Drugs were obtained from Sigma or Tocris (except for TTX, from Alamone Labs). Recordings were made using two Axopatch 200B amplifiers or a single MultiClamp 700A amplifier (Axon Instruments). Currents were elicited at 15- to 40-s intervals, low-pass filtered at 2 kHz, and digitized at 10 kHz by an Instrutech ITC-18 A/D board controlled by software written for Igor Pro (WaveMetrics). Presynaptic currents were leak-subtracted (P/4 protocol). Data analysis was performed using Igor Pro and Excel

Address for reprint requests and other correspondence: J. H. Singer, Departments of Ophthalmology and Physiology, Northwestern University Feinberg School of Medicine, 303 E. Chicago Ave., Tarry 5-715, Chicago, IL 60611 (E-mail: j-singer@northwestern.edu).

The costs of publication of this article were defrayed in part by the payment of page charges. The article must therefore be hereby marked "*advertisement*" in accordance with 18 U.S.C. Section 1734 solely to indicate this fact.

(Microsoft). To estimate the size of the RRP, we first deconvolved the quantal miniature excitatory postsynaptic current (mEPSC) waveform from the EPSC (Singer et al. 2004). Then we subtracted a single exponential function, $f(t) = a[1 - e^{(-t/\tau)}]$, where $a$ is the steady-state amplitude of the EPSC and $\tau$ is the time constant of the decay of the deconvolved waveform from the EPSC, and integrated the remaining current (Fig. 1). The integral was divided by the charge transfer of the average quantal mEPSC to yield the total number of vesicles released during the transient portion of the EPSC, i.e., the RRP. Paired, two-tailed *t*-tests were used to compare data sets. In all cases, significance was accepted as $P < 0.05$. Unless indicated otherwise, data are presented as means ± SE, and illustrated traces are averages of five to ten responses.

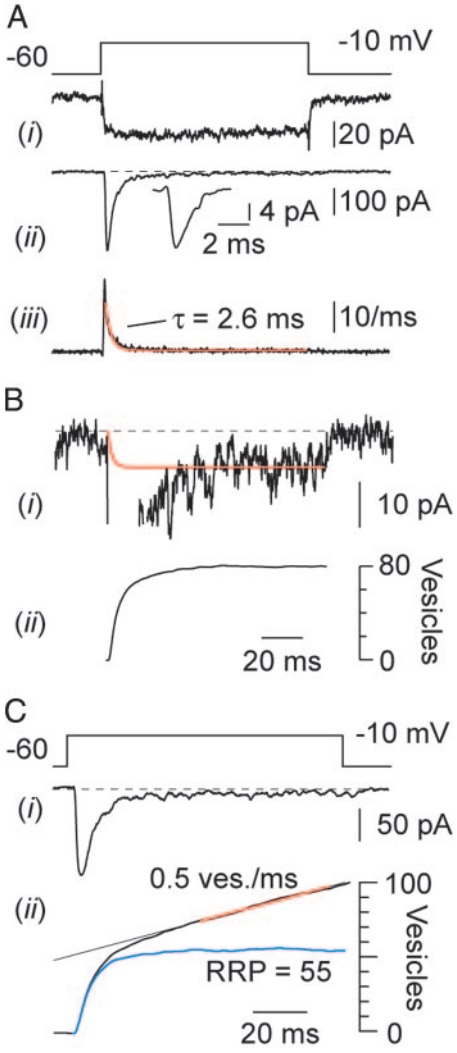


FIG. 1. Estimating the readily releasable pool (RRP) size. *A*: stepping the presynaptic rod bipolar cell (RBC) to −10 mV for 100 ms elicits a presynaptic $Ca^{2+}$ current (*i*) and evokes an excitatory postsynaptic current (EPSC) (*ii*) constituting a large, transient component and a small, sustained component. When the quantal miniature (m-)EPSC (*ii*, *inset*) is deconvolved from the EPSC waveform, the instantaneous release rate can be estimated (*iii*). On average, the release rate declines exponentially with $\tau = 4.1 \pm 0.3$ ms ($n = 27$). For the illustrated recording, $\tau = 2.6$ ms (*red trace*). *B*: a decaying exponential function (*red trace*), with a $\tau$ equivalent to that of the deconvolved waveform and amplitude equal to that of the steady-state EPSC amplitude, is subtracted from the EPSC (*i*). *Difference trace* is integrated and normalized to the mEPSC integral (*ii*), reflecting the release of the RRP. *C*: a 100-ms step to −10 mV evokes an EPSC (*i*). Presynaptic $Ca^{2+}$ current is omitted for simplicity. When the EPSC is integrated and normalized to the mEPSC integral (*iii*, *black trace*), the integrated trace is linear during the steady-state component of the EPSC (*red trace*). Slope of this portion of the curve is 0.47 vesicles/ms for this recorded RBC–AII pair and 0.53 ± 0.06 vesicles/ms for $n = 27$ recorded pairs. Also shown (*iii*) is the release of the RRP for this recorded pair (*blue trace*).

## RESULTS

### *Estimating the RRP size*

Paired, voltage-clamp recordings were made from visually identified, synaptically coupled RBCs and AIIs as described previously (Singer and Diamond 2003). RBCs were stepped from a $V_m$ of −60 to −10 or 0 mV for 100 ms (Fig. 1*A*). This voltage step elicited a presynaptic current reflecting the activation of L-type $Ca^{2+}$ channels in the presynaptic terminal (Fig. 1*Ai*; also Singer and Diamond 2003) and evoked α-amino-3-hydroxy-5-methyl-4-isoxazolepropionic acid receptor (AMPAR)–mediated EPSCs that exhibited two distinct components (Fig. 1*Aii*). The first was fast, rising in about 1 ms and decaying within 10 ms, giving rise to the EPSC peak. The second was sustained, arising from small synaptic events that persisted throughout the remainder of the depolarization. We postulate that the rapid decay of the large, initial component reflects release from and subsequent depletion of the RRP, and that the small, sustained component reflects equilibrium between release from and replenishment of the RRP (also Mennerick and Matthews 1996).

Because the postsynaptic AMPARs on AIIs act as linear detectors of exocytosis, the release rate at the RBC terminal may be derived by deconvolving the quantal mEPSC waveform from the EPSC (Singer and Diamond 2003; Singer et al. 2004; Fig. 1). During a 100-ms presynaptic depolarization, the rate of release declined exponentially after the EPSC peak (Fig. 1*Aiii*: $\tau = 4.1 \pm 0.3$ ms; $n = 27$); this decrease reflects the emptying of the RRP. This value is comparable to the time constant of RRP depletion measured at calyceal synapses in the auditory brain stem (2.9 ms: Sun and Wu 2001) and to that calculated from capacitance measurements from isolated goldfish Mb1 terminals (1.5 ms: Mennerick and Matthews 1996; 3.6 ms: Gomis et al. 1999).

To estimate the initial size of the RRP, we integrated the fast component of the EPSC (Fig. 1*Bi*; see METHODS for details). This fast component was isolated by subtracting a waveform with an exponential rise equivalent to the decay of the deconvolved waveform and an amplitude equivalent to the steady-state component of the EPSC from the EPSC. This waveform represented the steady, relatively slow replenishment of the RRP that begins as depletion progresses. With this method, we found that the RRP was composed of 70 ± 7 vesicles ($n = 27$; Fig. 1*Bii*). Previous work indicates that RBC–AII pairs are connected by, on average, 10 ribbon synapses (Singer et al. 2004), suggesting that the RRP at each ribbon is about 70 ÷ 10 = 7 vesicles (the number of vesicles tethered to a single mammalian bipolar cell ribbon has not been reported; see DISCUSSION). If the sustained component of the EPSC reflects equilibrium between release from and replenishment of the RRP, we can estimate the refilling rate of the RRP during ongoing exocytosis. To do this, we integrated the EPSC and measured the slope of the integral during the period corresponding to the steady-state component (Fig. 1*C*); it was 0.53 ± 0.06 vesicles/ms ($n = 27$). At an individual synapse,

then, the steady-state release rate was about 50 Hz: i.e., 0.53 vesicles/ms ÷ 10 synapses.

### *Receptor desensitization does not affect measurement of the RRP*

Our approach to estimating the RRP size and the steady-state release rate requires that the EPSC reflect accurately presynaptic exocytosis without any effect of postsynaptic AMPAR desensitization. Two sets of experimental results indicate that this requirement is met at RBC–AII synapses: *1*) the amplitude of individual synaptic events did not vary throughout the duration of steady-state release (Fig. 2, *A* and *B*); and *2*) blocking AMPAR desensitization with cyclothiazide (CTZ; 50 $\mu$M) equally affected the steady-state postsynaptic current and spontaneous, quantal mEPSCs (Fig. 2, *C–E*).

To determine whether postsynaptic AMPARs were desensitized significantly after the transient component of the EPSC (and the release of the RRP), we looked for time-dependent changes in individual synaptic events during the last 80 ms of an EPSC evoked by a 100-ms presynaptic depolarization. If significant desensitization occurred, the amplitudes of individual synaptic events occurring early in the steady-state condition would have been attenuated by desensitization, and this effect would have diminished over time as AMPARs recovered from desensitization (Otis et al. 1996). This analysis was possible only in a subset of paired recording experiments in which synaptic events could be isolated and measured accurately (i.e., the rate of release was not so high that individual synaptic currents could not be resolved; Fig. 2*A*). Individual event amplitudes were measured, normalized to the average quantal mEPSC amplitude measured in the same cell, and binned at 10-ms intervals (Fig. 2*B*; $n = 11$). Event amplitudes in the first bin were statistically indistinguishable from those in the last ($P = 0.22$; $n = 11$), indicating that postsynaptic responses were not reduced transiently by receptor desensitization. Interestingly, these evoked synaptic events were larger than quantal mEPSCs (average quantal content = 1.3 ± 0.3, $n = 11$), consistent with previous descriptions of coordinated multivesicular release at this synapse (Singer et al. 2004).

Blocking AMPAR desensitization with CTZ increased both the peak and steady-state amplitudes of EPSCs (to 135 ± 7 and 538 ± 41% of control, respectively; $n = 11$; Fig. 2, *C* and *D*). Also, CTZ increased the amplitudes and slowed the decay of quantal mEPSCs (Fig. 2*C*, *inset*, and Fig. 2*E*; also Singer and Diamond 2003), as a result of its enhancement of AMPAR affinity (Partin et al. 1994, 1996; Patneau et al. 1993; Yamada and Tang 1993). The effect of CTZ on mEPSC charge transfer (increased to 496 ± 33% of control, $n = 11$) was not significantly different from its effect on the steady-state component of the EPSC ($P = 0.20$; Fig. 2*E*), indicating that receptor desensitization does not diminish postsynaptic AMPAR sensitivity during a step-evoked EPSC. The smaller effect of CTZ on the peak of the step-evoked EPSC compared with that of the mEPSC likely indicates that, in the presence of CTZ, postsynaptic receptors are saturated at the peak of the step-evoked EPSC. Results described below, however, indicate that receptor saturation does not occur during step-evoked EPSCs in the

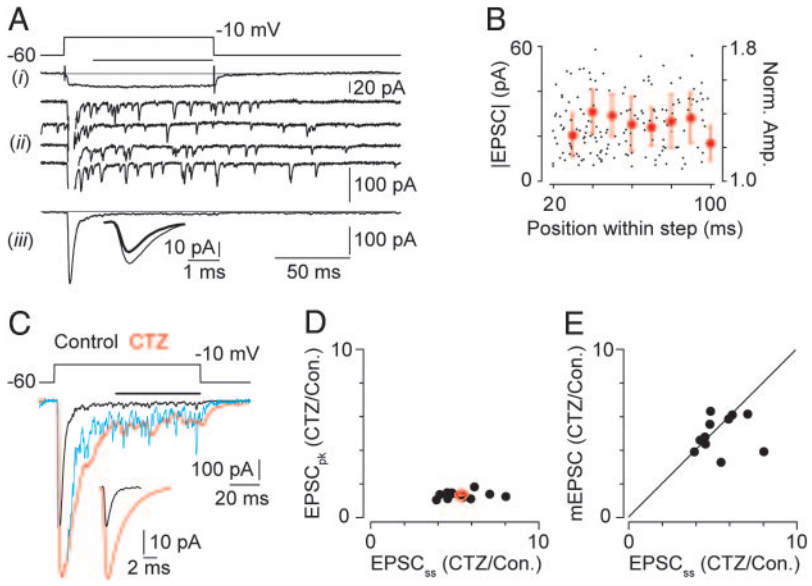


FIG. 2. EPSCs are unaffected by $\alpha$-amino-3-hydroxy-5-methyl-4-isoxazolepropionic acid receptor (AMPAR) desensitization. *A*: a 100-ms presynaptic voltage step to −10 mV evokes a sustained presynaptic $Ca^{2+}$ current (*i*) and compound EPSCs in which individual release events can be discerned during the steady-state component. Single responses, with the peaks blanked out, are shown in (*ii*) and the average EPSC in (*iii*). Individual evoked events occurring during the last 80 ms of the EPSC (black bar) are slightly larger than quantal mEPSCs (*inset*; average mEPSC is *thick trace*). *B*: amplitudes of individual synaptic events are independent of their temporal position within the compound postsynaptic response; 160 synaptic events from a single recording are illustrated (black dots); superimposed are averaged, binned data from $n = 11$ paired recordings (red circles). Amplitudes of the events in the first and last bins are statistically indistinguishable ($P = 0.22$). *C*: EPSCs evoked by a 100-ms step from −60 to −10 mV (the presynaptic $Ca^{2+}$ current is omitted for simplicity) in control (black) and CTZ (50 $\mu$M)-containing external solutions. When the control EPSC is scaled by the ratio of the mEPSC integrals in cyclothiazide (CTZ) and control conditions (about 6:1; *cyan trace*), the steady-state amplitudes (black bar) of the scaled EPSC and the EPSC in CTZ are approximately the same. *Inset*: average mEPSCs. *D*: effect of CTZ on the steady-state EPSC is plotted against its effect on the EPSC peak. Results from individual experiments (black) and the average of $n = 11$ experiments (red) are illustrated. CTZ affects the steady-state amplitude to a much greater extent than the peak amplitude (to 135 ± 5 vs. 538 ± 41% of control, respectively). *E*: effect of CTZ on the steady-state EPSC is plotted against its effect on the mEPSC charge transfer. Two effects are approximately equivalent (to 538 ± 41 vs. 496 ± 33% of control, respectively), and results from $n = 11$ paired recordings are clustered along the unity line.

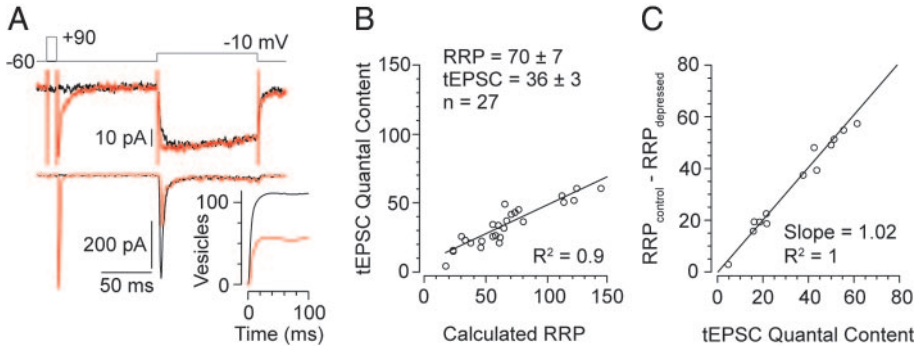


FIG. 3. Vesicle depletion is the primary cause of short-term depression. *A*: a step to −10 mV (*black traces*) was preceded in alternate trials (*red traces*) by a $Ca^{2+}$ tail current. tEPSC depresses the step-evoked response. *Inset*: calculated RRP size before (black) and after (red) depression by the tEPSC. *B*: quantal content of the tEPSC varies linearly with the calculated RRP size. For $n = 27$ cell pairs, the RRP was calculated to be 70 ± 7 vesicles, and the average quantal content of the tEPSC = 36 ± 3 quanta, equivalent to 54 ± 3% of the RRP. *C*: RRP is reduced by the number of vesicles released by the depressing stimulus: plotted is the calculated quantal content of the tEPSC against the difference in the calculated RRP.

absence of CTZ (Fig. 3). We conclude, then, that the EPSC waveform is an accurate description of the time course of presynaptic exocytosis (see also Singer and Diamond 2003).

### *Evidence for depletion during PPD*

Eliciting $Ca^{2+}$ entry into the RBC terminal with a $Ca^{2+}$ tail current evokes a large fast EPSC that we call a *tEPSC* (Fig. 3*A*; also Singer and Diamond 2003). Paired tEPSCs evoked at short intervals show pronounced paired-pulse depression (PPD) that is presynaptic in origin (Singer et al. 2004; also Fig. 4*A*). The second tEPSC is reduced by about 60%, which is similar to the reduction of the release probability of individual release sites ($p$) during PPD (53%), as determined by quantal analysis (Singer et al. 2004). If vesicle depletion were the primary cause of PPD, then the quantal content of a tEPSC should constitute a similar fraction (53–60%) of the RRP.

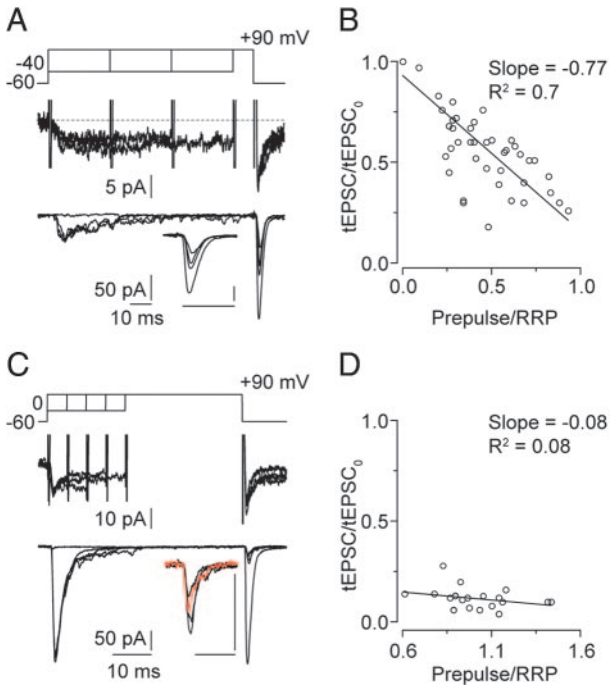


FIG. 4. Increasing release from the RRP enhances short-term depression. *A*: tEPSCs were evoked after voltage steps of increasing duration (0, 30, 60, and 90 ms) to −40 mV. As the duration of the prepulses was increased, the amplitudes of the tEPSCs decreased. *Inset*: tEPSCs illustrated at higher temporal resolution. *B*: relationship between tEPSC depression and the number of vesicles released from the RRP is linear, with a slope close to 1. RRP was calculated by scaling the quantal content of the tEPSC by 1.85. Quantal contents of depressed tEPSCs are normalized to those of the tEPSCs in the absence of prepulses. *C*: tEPSCs were evoked after voltage steps of increasing duration (0, 10, 20, 30, 40 ms) to 0 mV. Increasing the duration of these RRP-depleting prepulses did not increase the extent of tEPSC depression. *Inset*: depressed tEPSCs alone are illustrated; the *red trace* is the tEPSC after the longest (40 ms) prepulse. *D*: amplitude of the depressed tEPSC is relatively constant after RRP depletion (RRP calculated as in *B*). Line fit to the data has a slope close to 0.

To test this prediction, we measured the RRP size before and 100 ms after inducing synaptic depression with a tEPSC (Fig. 3*A*). For the RBC–AII pairs in which we recorded both tEPSCs and estimated the RRP size ($n = 27$), the quantal content of the tEPSC was 36 ± 3 vesicles, or 54 ± 3% of the RRP (Fig. 3*B*). When tEPSCs were evoked 100 ms before a step-evoked EPSC on alternate trials, the tEPSC depressed the amplitude of the EPSC. Calculating the size of the remainder of the RRP from this EPSC yielded a value that was 46 ± 3% of the original. Because a tEPSC reduced the RRP to nearly the same extent as the change in $p$ during PPD (Singer et al. 2004), synaptic depression at this synapse likely results primarily from vesicle depletion. Additionally, the correspondence between the quantal content of the tEPSC the subsequent reduction in RRP size (Fig. 3*C*) confirms the accuracy of our approach to measuring the RRP size and indicates that postsynaptic AMPARs are not saturated by glutamate during the peaks of the tEPSC and the subsequent step-evoked EPSC in the absence of CTZ.

If vesicle depletion were the primary cause of synaptic depression, the extent of depression should vary linearly with the number of vesicles released from the RRP by a nondepleting stimulus. To test this hypothesis, we examined the amplitude of tEPSCs evoked after small presynaptic depolarizations of varying length (steps from −60 to −40 mV for 10–90 ms; Fig. 4*A*). As expected, the extent of tEPSC depression increased as the prepulse was lengthened (Fig. 4*A*). We estimated the RRP size by dividing the quantal content of the tEPSC by 0.54, based on the close correlation between the tEPSC quantal content and RRP (Fig. 3*B*). When the normalized amplitude of the depressed tEPSC was plotted against the fraction of the RRP released by the prepulse, a linear relationship was observed (Fig. 4*B*; $n = 12$), indicating that fractional depletion of the RRP causes a nearly proportional decrease in the tEPSC quantal content and supporting the conclusion that vesicle depletion underlies short-term depression at RBC synapses. That the fractional reduction in tEPSC quantal content was slightly smaller than that in the RRP may indicate that the RRP is replenished to a small extent during the step depolarization.

After depletion of the RRP during the first few milliseconds of prolonged presynaptic depolarization (e.g., a 100-ms step from −60 to −10 mV as in Fig. 1*A*), exocytosis occurs at a low

rate (0.5 vesicles/ms; Fig. 1*C*) that reflects equilibrium between release from and replenishment of the RRP. Consequently, the tEPSC quantal content is not reduced to zero by prepulses that release the RRP in its entirety (Fig. 4*B*). This is illustrated clearly by recordings in which strong presynaptic depolarizations of increasing length (steps from −60 to 0 mV for 5–50 ms) are used as prepulses (Fig. 4*C*). Here, evoking the release of more vesicles than were contained initially in the RRP does not reduce the quantal content of the tEPSC further than the release of the RRP alone (Fig. 4*D*; $n = 5$). The ratio of the depressed tEPSC to the control tEPSC was 0.15 ± 0.04 after a 5-ms prepulse and 0.12 ± 0.02 after a 20-ms prepulse; these differences were not statistically significant ($P = 0.62$; $n = 5$). Because the amplitude of the depressed tEPSC does not vary with the duration of steady-state release, *p* likely is not changed significantly during synaptic depression.

### *Depression and recovery of tEPSCs*

The experiments illustrated in Figs. 2–4 indicate that paired-pulse depression occurring at short interpulse intervals is profound (from about 70–85%, depending on the magnitude of the depressing stimulus). This is consistent with previous observations that paired tEPSCs evoked at 25- to 100-ms intervals exhibit pronounced PPD, independent of postsynaptic receptor desensitization, accompanied by a reduction in multivesicular release (Singer et al. 2004). We measured the rate of recovery of tEPSCs from PPD by increasing the paired-pulse interval from 15 ms to 15.1 s in logarithmic increments (Fig. 5*A*) and determined that its time course was slow and monoexponential, with $\tau = 3.9$ s (Fig. 5*C*; $n = 7$). To eliminate any effects of exogenous buffers on presynaptic $Ca^{2+}$ dynamics, RBCs were recorded in the perforated-patch configuration

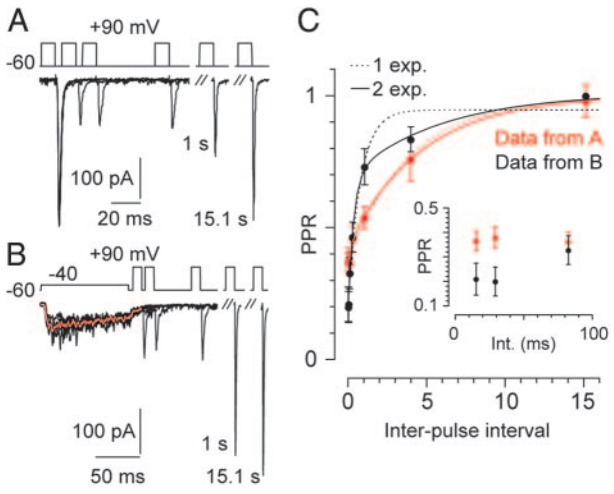


FIG. 5. Recovery from paired-pulse depression (PPD) is slow. *A*: paired tEPSCs, elicited at increasing intervals, show PPD that is slow to recover. *B*: recovery of the tEPSC from depression is faster when a voltage step (100 ms to −40 mV) is the depressing stimulus. Average step-evoked EPSC is illustrated in red, and the average quantal content of this EPSC is 159 ± 23% of the RRP ($n = 7$). *C*: illustrated is the summary of the time course of recovery. In the experiments exemplified by *A*, recovery from PPD is slow and monoexponential (red): $\tau = 3.9$ s ($n = 7$). *Inset*: no recovery occurs in the first 100 ms after the initial response (red circles). In the experiments exemplified by *B*, recovery is faster and biexponential: $\tau_{fast} = 0.4$ s (40%), $\tau_{slow} = 5.9$ (60%), $\tau_{mean} = 2.6$ s ($n = 7$). *Inset*: recovery begins after about 30 ms (black circles).

during these experiments. No recovery from PPD was apparent within the first 100 ms of the first pulse (Fig. 5*C*, *inset*; PPR = 0.38 ± 0.1 for 15-ms intervals and 0.36 ± 0.1 for 82.32-ms intervals; see also Gomis et al. 1999). This slow recovery is comparable to that measured with capacitance measurements of fast exocytosis from isolated goldfish Mb1 bipolar cell terminals ($\tau \approx 4$ s; Mennerick and Matthews 1996).

At other synapses, the rate of recovery from use-dependent depression varies with the frequency of presynaptic stimulation, and this has been interpreted to reflect the $Ca^{2+}$ dependency of this process (Dittman and Regehr 1998; Kusano and Landau 1975; Stevens and Wesseling 1998; Wang and Kaczmarek 1998). We tested next whether recovery from PPD at RBC ribbon synapses was altered after sustained exocytosis. We elicited $Ca^{2+}$ tail currents at increasing intervals after the end of a 100-ms step to −40 mV. This level of sustained depolarization is in the physiological operating range of mammalian rod bipolar cells (−45 to −30 mV; e.g., Euler and Masland 2000) and it elicited small, sustained presynaptic $Ca^{2+}$ currents that evoked a relatively small, slow EPSC (Fig. 5*B*). On average, this EPSC reflected release of 159 ± 23% of the RRP (estimated by dividing the quantal content of the tEPSC by 0.54, as described above), indicating that release, replenishment, and subsequent release events occur at individual sites during the EPSC. A tEPSC evoked 15 ms after the step-evoked EPSC was reduced in amplitude relative to a control tEPSC evoked 17 s later: PPR = 0.21 ± 0.07. When the tEPSC was depressed by this step-evoked EPSC, a fast component of recovery was revealed, and the time course of recovery was well fit by a double-exponential curve ($\tau_{mean} = 2.6$ s; Fig. 5*C*). At an interstimulus interval of 1,024 ms, the tEPSC had recovered to 73 ± 7% of its control amplitude, whereas the tEPSC depressed by a tEPSC had recovered to only 46 ± 6% of its control amplitude; this difference is statistically significant ($P = 0.02$ by ANOVA; $n = 7$). Because increasing the duration of $Ca^{2+}$ entry during the depressing stimulus accelerated the recovery of the tEPSC amplitude, we conclude that vesicle replenishment at RBC synapses is enhanced after sustained exocytosis.

## DISCUSSION

### *Measuring the size of the RRP*

We estimated the size of the RRP of vesicles in RBC terminals by integrating the initial component of the EPSC evoked in postsynaptic AII amacrine cells by a 100-ms presynaptic voltage step (Fig. 1). We postulated that the rapid decay of this initial component reflected the depletion of vesicles from the RRP and that the later, sustained component of the EPSC reflected a steady-state condition in which vesicles were released from the RRP shortly after they were delivered into it. Our measurements indicate that the RRP at a single presynaptic active zone (i.e., on a single ribbon) is about seven vesicles, assuming 10 synaptic contacts between a single RBC and a single AII (Singer et al. 2004).

At some synapses, postsynaptic measurement of the RRP is complicated by receptor desensitization and saturation (Neher and Sakaba 2001a). AMPAR desensitization does not appear to compromise our measurements of the RRP at RBC ribbon synapses: the amplitude of evoked synaptic events does not

change during sustained exocytosis (Fig. 2, *A* and *B*), and blocking AMPAR desensitization does not change the apparent quantal content of the steady-state component of the step-evoked EPSC (Fig. 2, *C* and *D*). AMPARs in AIIs exhibit rapid deactivation kinetics and recorded mEPSCs decay with a $\tau < 1$ ms (Morkve et al. 2002; Singer and Diamond 2003; Veruki et al. 2003). Desensitization of these receptors is slow relative to deactivation (the predominant $\tau_{desens.} = 3.5$ ms and $\tau_{deact.} = 1.1$ ms), and recovery from desensitization is fast ($\tau = 12.5$ ms) (Veruki et al. 2003). Thus postsynaptic AMPARs are likely not desensitized significantly during the sustained component of the EPSC, when the release rate is relatively low. Additionally, the PPR of two tEPSCs is unaffected by CTZ, indicating that the AMPARs are not desensitized strongly after the initial, fast component of the EPSC (Singer et al. 2004).

At some synapses, high $p$ or slowed glutamate clearance leads to postsynaptic AMPAR saturation and sublinear summation of presynaptic activity (Foster et al. 2002; Harrison and Jahr 2003; Neher and Sakaba 2001b; Wadiche and Jahr 2001). Multivesicular events at individual RBC–AII synapses, however, obey simple binomial statistics (Singer et al. 2004), indicating that AMPARs at this synapse respond linearly to changes in cleft (glutamate). Moreover, enhancing AMPAR affinity with CTZ does not affect the PPR of two tEPSCs (Singer et al. 2004). Here, we found the fractional depletion (by 54 ± 3%) of the RRP by a tEPSC to be in close correspondence with the ratio of their quantal contents (tEPSC = 54 ± 3% of the RRP; Fig. 3). The agreement between these values attests to the accuracy of our RRP measurements. As we have estimated previously that a single RBC makes approximately 10 synapses onto a single AII (Singer et al. 2004), the RRP at each ribbon synapse constitutes seven vesicles on average, similar to the RRP size (i.e., the number of docked vesicles visualized in serial EM sections) at conventional hippocampal and cerebellar synapses (e.g., Schikorski and Stevens 1997; Xu-Friedman et al. 2001) but about 50% smaller than that at Mb1 ribbon synapses (von Gersdorff et al. 1996; but see Sterling and Matthews 2005).

### *Estimating the refilling rate at a single release site*

The ratio between the total number of vesicles tethered to a retinal synaptic ribbon and the number of tethered vesicles that are also docked at the plasma membrane is 5:1 (Sterling and Matthews 2005). Because the RRP at such synapses is thought to constitute the bottom row of vesicles on either side of the ribbon (von Gersdorff et al. 1996), we anticipate that the mammalian RBC ribbon should tether about $7 \times 5 = 35$ vesicles. To our knowledge, however, such measurements have not been reported.

Once vesicles are released from the RRP, release sites are refilled from a recycling pool (Rizzoli and Betz 2005); it has been suggested that the ribbon serves as the site at which recycling vesicles are located (Parsons and Sterling 2003; von Gersdorff et al. 1996). In goldfish Mb1 terminals, the recycling pool is nearly twice the size of the RRP (Gomis et al. 1999) and, at conventional vertebrate synapses, the recycling pool of vesicles is two- to fourfold larger than the RRP (Rizzoli and Betz 2005), similar to the relationship between the relative number of ribbon-associated vesicles and the RRP (von Gersdorff et al. 1996). We measured the refilling rate of the RRP during ongoing release (i.e., during the sustained component of the EPSC) as 0.53 $ms^{-1}$ (Fig. 1*C*). Each of 70 release sites, then, is refilled at a rate of $0.53 \div 70 = 0.008$ $ms^{-1}$, which corresponds to a recovery time constant of 132 ms. This is comparable to the rate of continuous exocytosis measured from isolated Mb1 terminals (Lagnado et al. 1996; Neves and Lagnado 1999; Rouze and Schwartz 1998). This suggests that >95% of the vesicles on the mammalian RBC ribbon can be released in about 500 ms ($3\tau = 496$ ms), consistent with measurements made from isolated Mb1 terminals (Heidelberger et al. 2002; Mennerick and Matthews 1996; von Gersdorff et al. 1996). In making these comparisons, however, it is important to note that mammalian and goldfish ribbon synapses may be optimized to operate at different temperatures.

Release sites are refilled more slowly in the absence of continuous exocytosis: during recovery from PPD the PPR of two tEPSCs recovers with a time constant of 3.9 s (Fig. 5, *A* and *C*). Recovery is faster (weighted $\tau = 2.6$ s) when the tEPSC is depressed by a step-evoked EPSC rather than a tEPSC (Fig. 5, *B* and *C*), indicating that the refilling rate is $Ca^{2+}$ sensitive; in the absence of exocytotic activity, the refilling rate of the release sites is relatively low. This is in keeping with a study demonstrating that $Ca^{2+}$ modulates the rate of RRP refilling in Mb1 terminals (Gomis et al. 1999). The difference in recovery could reflect activity-dependent changes in either endocytotic or exocytotic pathways.

### *Depletion versus other mechanisms of synaptic depression*

In the simplest model of synaptic depression arising from vesicle depletion (reviewed by Zucker and Regehr 2002), a brief presynaptic stimulus releases a constant fraction (F) of the RRP, and the quantal content of a single EPSC is F × RRP. When paired stimuli are delivered within a short interval to preempt RRP replenishment, PPR = 1 − F. Here, we found that a single tEPSC reflects the release of a consistent fraction (54%) of the measured RRP (Fig. 3*B*). In the simplest depletion model, then, the PPR of two closely spaced (<100-ms interpulse interval) tEPSCs would be 0.46, which is slightly greater that the experimentally measured PPR of about 0.4 (Fig. 5; Singer et al. 2004).

Discrepancies between PPD predicted by the simple depletion model and PPD measured experimentally have given rise to the suggestion that F may be variable (see Zucker and Regehr 2002). Such variability in F may arise from use-dependent changes in $p$, reflecting a reduction in the efficiency of exocytosis, as has been suggested to occur at conventional synapses (Bellingham and Walmsley 1999; Betz 1970; Burrone and Lagnado 2000; Hsu et al. 1996; Wu and Borst 1999) and isolated Mb1 ribbon synapses (Burrone and Lagnado 2000). Given the close correlation between the number of vesicles released from the RRP and the reduction in the quantal content of EPSCs during synaptic depression (Figs. 3 and 4), however, it is evident that vesicle depletion is the primary cause of short-term depression at mammalian RBC synapses.

### *Contribution of depression to retinal processing*

By matching its gain to the ambient light intensity, a process known generally as adaptation, the retina can encode changes in light intensity over 12 orders of magnitude without saturat-

ing the limited dynamic ranges of individual neurons (reviewed by Shapley 1997; Shapley and Enroth-Cugell 1984). Adaptation occurs in both the phototransduction cascade (Baylor et al. 1980; Nakatani et al. 1991) and in neural circuits within the inner retina (Barlow and Levick 1969; Dowling 1967; Frishman and Sieving 1995; Frishman et al. 1996), but during rod vision, neural adaptation is apparent at light intensities too low to cause adaptation of rod phototransduction (Barlow and Levick 1969; Enroth-Cugell and Shapley 1973; Frishman and Sieving 1995; Naarendorp et al. 2001; Saszik et al. 2002). Although the mechanisms underlying neural adaptation are largely unknown, synaptic depression is an excellent candidate because it allows synaptic strength to vary with the activity history of the presynaptic neurons. In the auditory brain stem, synaptic depression is thought to allow interaural timing differences to be preserved as sound intensity increases by minimizing steady-state changes in firing rate (Cook et al. 2003).

Although most studies of scotopic vision focus on the rod pathway's ability to transfer with high-fidelity small photoreceptor responses to ganglion cells, scotopic vision also requires motion detection, and thus temporal information must be encoded by the rod pathway (Field et al. 2005). Light responses of mammalian RBCs are faster than those of rods (Field and Rieke 2002), and those of ganglion cells are faster still (e.g., see Fig. 6*B* in Field et al. 2005). It has been suggested that AII amacrine cells serve to "quicken" rod signaling (Nelson 1982), indicating that the intrinsic properties of RBC synapses make an important contribution to temporal processing in the mammalian rod circuit. Our previous work has demonstrated that the time course of exocytosis from RBC terminals is inherently transient (Singer and Diamond 2003). Here, we find that this likely reflects the small size of the RRP at RBC ribbon synapses. This relatively small RRP and a high $p$ ensure that short-term depression arising from vesicle depletion limits sustained neurotransmission, contributing to the transient signaling characteristic of the inner retina. Electrophysiological and computational studies of cortical networks indicate that synaptic depression allows postsynaptic neurons to respond preferentially to changes in presynaptic firing rate rather than the absolute value of the firing rate (Abbott et al. 1997; Tsodyks and Markram 1997), suggesting that synaptic depression is a general mechanism that promotes transient signaling throughout the CNS.

## GRANTS

This work was supported by the National Institute of Neurological Disorders and Stroke intramural research program and by NS-43365 to J. H. Singer.

## REFERENCES

**Abbott LF, Varela JA, Sen K, and Nelson SB.** Synaptic depression and cortical gain control. *Science* 275: 220–224, 1997.

**Barlow HB and Levick WR.** Three factors limiting the reliable detection of light by retinal ganglion cells of the cat. *J Physiol* 200: 1–24, 1969.

**Baylor DA, Matthews G, and Yau KW.** Two components of electrical dark noise in toad retinal rod outer segments. *J Physiol* 309: 591–621, 1980.

**Bellingham MC and Walmsley B.** A novel presynaptic inhibitory mechanism underlies paired pulse depression at a fast central synapse. *Neuron* 23: 159–170, 1999.

**Betz WJ.** Depression of transmitter release at the neuromuscular junction of the frog. *J Physiol* 206: 629–644, 1970.

**Burrone J and Lagnado L.** Synaptic depression and the kinetics of exocytosis in retinal bipolar cells. *Neuroscience* 20: 568–578, 2000.

**Cook DL, Schwindt PC, Grande LA, and Spain WJ.** Synaptic depression in the localization of sound. *Nature* 421: 66–70, 2003.

**Dittman JS and Regehr WG.** Calcium dependence and recovery kinetics of presynaptic depression at the climbing fiber to Purkinje cell synapse. *Neuroscience* 18: 6147–6162, 1998.

**Dowling JE.** The site of visual adaptation. *Science* 155: 273–279, 1967.

**Enroth-Cugell C and Shapley RM.** Adaptation and dynamics of cat retinal ganglion cells. *J Physiol* 233: 271–309, 1973.

**Euler T and Masland RH.** Light-evoked responses of bipolar cells in a mammalian retina. *J Neurophysiol* 83: 1817–1829, 2000.

**Field GD and Rieke F.** Nonlinear signal transfer from mouse rods to bipolar cells and implications for visual sensitivity. *Neuron* 34: 773–785, 2002.

**Field GD, Sampath AP, and Rieke F.** Retinal processing near absolute threshold: from behavior to mechanism. *Annu Rev Physiol* 67: 491–514, 2005.

**Foster KA, Kreitzer AC, and Regehr WG.** Interaction of postsynaptic receptor saturation with presynaptic mechanisms produces a reliable synapse. *Neuron* 36: 1115–1126, 2002.

**Frishman LJ, Reddy MG, and Robson JG.** Effects of background light on the human dark-adapted electroretinogram and psychophysical threshold. *J Opt Soc Am A Opt Image Sci Vis* 13: 601–612, 1996.

**Frishman LJ and Sieving PA.** Evidence for two sites of adaptation affecting the dark-adapted ERG of cats and primates. *Vision Res* 35: 435–442, 1995.

**Gomis A, Burrone J, and Lagnado L.** Two actions of calcium regulate the supply of releasable vesicles at the ribbon synapse of retinal bipolar cells. *Neuroscience* 19: 6309–6317, 1999.

**Harrison J and Jahr CE.** Receptor occupancy limits synaptic depression at climbing fiber synapses. *Neuroscience* 23: 377–383, 2003.

**Heidelberger R, Sterling P, and Matthews G.** Roles of ATP in depletion and replenishment of the releasable pool of synaptic vesicles. *J Neurophysiol* 88: 98–106, 2002.

**Hsu SF, Augustine GJ, and Jackson MB.** Adaptation of Ca(2+)-triggered exocytosis in presynaptic terminals. *Neuron* 17: 501–512, 1996.

**Kusano K and Landau EM.** Depression and recovery of transmission at the squid giant synapse. *J Physiol* 245: 13–22, 1975.

**Lagnado L, Gomis A, and Job C.** Continuous vesicle cycling in the synaptic terminal of retinal bipolar cells. *Neuron* 17: 957–967, 1996.

**Mennerick S and Matthews G.** Ultrafast exocytosis elicited by calcium current in synaptic terminals of retinal bipolar neurons. *Neuron* 17: 1241–1249, 1996.

**Morkve SH, Veruki ML, and Hartveit E.** Functional characteristics of non-NMDA-type ionotropic glutamate receptor channels in AII amacrine cells in rat retina. *J Physiol* 542: 147–165, 2002.

**Naarendorp F, Sato Y, Cajdric A, and Hubbard NP.** Absolute and relative sensitivity of the scotopic system of rat: electroretinography and behavior. *Vis Neurosci* 18: 641–656, 2001.

**Nakatani K, Tamura T, and Yau KW.** Light adaptation in retinal rods of the rabbit and two other nonprimate mammals. *J Gen Physiol* 97: 413–435, 1991.

**Neher E and Sakaba T.** Combining deconvolution and noise analysis for the estimation of transmitter release rates at the calyx of held. *Neuroscience* 21: 444–461, 2001a.

**Neher E and Sakaba T.** Estimating transmitter release rates from postsynaptic current fluctuations. *Neuroscience* 21: 9638–9654, 2001b.

**Nelson R.** AII amacrine cells quicken time course of rod signals in the cat retina. *J Neurophysiol* 47: 928–947, 1982.

**Neves G and Lagnado L.** The kinetics of exocytosis and endocytosis in the synaptic terminal of goldfish retinal bipolar cells. *J Physiol* 515: 181–202, 1999.

**Otis T, Zhang S, and Trussell LO.** Direct measurement of AMPA receptor desensitization induced by glutamatergic synaptic transmission. *Neuroscience* 16: 7496–7504, 1996.

**Parsons TD and Sterling P.** Synaptic ribbon. Conveyor belt or safety belt? *Neuron* 37: 379–382, 2003.

**Partin KM, Fleck MW, and Mayer ML.** AMPA receptor flip/flop mutants affecting deactivation, desensitization, and modulation by cyclothiazide, aniracetam, and thiocyanate. *Neuroscience* 16: 6634–6647, 1996.

**Partin KM, Patneau DK, and Mayer ML.** Cyclothiazide differentially modulates desensitization of alpha-amino-3-hydroxy-5-methyl-4-isoxazolepropionic acid receptor splice variants. *Mol Pharmacol* 46: 129–138, 1994.

**Patneau DK, Vyklicky L Jr, and Mayer ML.** Hippocampal neurons exhibit cyclothiazide-sensitive rapidly desensitizing responses to kainate. *Neuroscience* 13: 3496–3509, 1993.

**Rizzoli SO and Betz WJ.** Synaptic vesicle pools. *Nat Rev Neurosci* 6: 57–69, 2005.

**Rouze NC and Schwartz EA.** Continuous and transient vesicle cycling at a ribbon synapse. *Neuroscience* 18: 8614–8624, 1998.

**Saszik SM, Robson JG, and Frishman LJ.** The scotopic threshold response of the dark-adapted electroretinogram of the mouse. *J Physiol* 543: 899–916, 2002.

**Schikorski T and Stevens CF.** Quantitative ultrastructural analysis of hippocampal excitatory synapses. *Neuroscience* 17: 5858–5867, 1997.

**Shapley R.** Retinal physiology: adapting to the changing scene. *Curr Biol* 7: R421–R423, 1997.

**Shapley RM and Enroth-Cugell C.** Visual adaptation and retinal gain controls. *Prog Retinal Res* 3: 263–346, 1984.

**Singer JH and Diamond JS.** Sustained $Ca^{2+}$ entry elicits transient postsynaptic currents at a retinal ribbon synapse. *Neuroscience* 23: 10923–10933, 2003.

**Singer JH, Lassova L, Vardi N, and Diamond JS.** Coordinated multivesicular release at a mammalian ribbon synapse. *Nat Neurosci* 7: 826–833, 2004.

**Sterling P and Matthews G.** Structure and function of ribbon synapses. *Trends Neurosci* 28: 20–29, 2005.

**Stevens CF and Wesseling JF.** Activity-dependent modulation of the rate at which synaptic vesicles become available to undergo exocytosis. *Neuron* 21: 415–424, 1998.

**Sun JY and Wu LG.** Fast kinetics of exocytosis revealed by simultaneous measurements of presynaptic capacitance and postsynaptic currents at a central synapse. *Neuron* 30: 171–182, 2001.

**Tsodyks MV and Markram H.** The neural code between neocortical pyramidal neurons depends on neurotransmitter release probability. *Proc Natl Acad Sci USA* 94: 719–723, 1997.

**Veruki ML, Morkve SH, and Hartveit E.** Functional properties of spontaneous EPSCs and non-NMDA receptors in rod amacrine (AII) cells in the rat retina. *J Physiol* 549: 759–774, 2003.

**von Gersdorff H, Vardi E, Matthews G, and Sterling P.** Evidence that vesicles on the synaptic ribbon of retinal bipolar neurons can be rapidly released. *Neuron* 16: 1221–1227, 1996.

**Wadiche JI and Jahr CE.** Multivesicular release at climbing fiber-Purkinje cell synapses. *Neuron* 32: 301–313, 2001.

**Wang LY and Kaczmarek LK.** High-frequency firing helps replenish the readily releasable pool of synaptic vesicles. *Nature* 394: 384–388, 1998.

**Wu LG and Borst JG.** The reduced release probability of releasable vesicles during recovery from short-term synaptic depression. *Neuron* 23: 821–832, 1999.

**Xu-Friedman MA, Harris KM, and Regehr WG.** Three-dimensional comparison of ultrastructural characteristics at depressing and facilitating synapses onto cerebellar Purkinje cells. *Neuroscience* 21: 6666–6672, 2001.

**Yamada KA and Tang CM.** Benzothiadiazides inhibit rapid glutamate receptor desensitization and enhance glutamatergic synaptic currents. *Neuroscience* 13: 3904–3915, 1993.

**Zucker RS and Regehr WG.** Short-term synaptic plasticity. *Annu Rev Physiol* 64: 355–405, 2002.